DAMAGE ARREST MECHANISMS IN NANOPARTICLE INTERLEAVED COMPOSITE INTERFACES

Nithya Subramanian [a], Chiara Bisagni [b]

a: Marie Sklodowska-Curie Postdoctoral Fellow, Aerospace Structures & Computational Mechanics, Faculty of Aerospace Engineering, Delft University of Technology, The Netherlands; n.subramanian-1@tudelft.nl

b: Professor, Aerospace Structures and Computational Mechanics, Faculty of Aerospace Engineering, Delft University of Technology, The Netherlands

Abstract: *The effectiveness of carbonaceous nanoparticles in arresting and delaying damage in nanocomposites has been attributed to multiscale toughening mechanisms. To explore their application in joined interfaces of composites, this study investigates the use of carbon nanotube (CNT) interleaved films for co-cured joining of composite parts and their consequent effects on the interfacial fracture toughness. Carbon nanotubes dispersed in a thermoset resin into thin films of two discrete thicknesses (200 μ and 500 μ) and three concentrations of CNT dispersion were chosen for this study (0.5% wt., 1% wt., and 2% wt.). The films were semi-cured in the oven before being incorporated as interleaves in the composite laminate interface. Fracture toughness of the interface in mode I loading conditions was determined through double cantilever beam (DCB). Micrographs of the fracture surfaces reveal a slip-and-stick based crack jump and arrest phenomena in mode I when nanoparticles are added to the interleaved interface. The thickness of the interleaves has a more significant effect on mode I toughening mechanisms than the concentration of the nanoparticles.*

Keywords: Co-cured composite interface; Interleaf; Carbon nanotubes; Fracture toughness

1. Introduction

Composite structures for aeronautical applications can be traditionally joined via adhesive co-bonding, co-curing, and/or mechanical fastening, which induce interfacial defects and stress concentrations under operational loads and increases structural weight. Co-cured joints, unlike co-bonded joints have no discernible interface due to diffusion of the adhesive into the laminate during cure [1,2]. However, controlling the flow of epoxy in the co-cure region as well as mitigating misalignment of the sub-components during co-cure are challenging and lead to irregularities. The incorporation of a partially cured epoxy film in the co-cured region ensures uniform thickness and restrains the relative sliding of the sub-components during co-cure, thus preventing misalignments. This technique also allows for an easier method to integrate the adhesive epoxy layer in the composite lay-up process.

Interleaved composite laminates with a discrete layer of epoxy films between joining surfaces have been studied as a strategy to improve damage tolerance during co-cured joining [3–5] and limit the need for accompanying mechanical fasteners. Owing to the presence of an interleaf film at the interface, larger damage zones arising from microcrack diffusion and crack path tortuosity are observed leading to higher interfacial fracture toughness [6]. Research over the past two decades has probed the effectiveness of dispersed and aligned carbonaceous

  doi:10.5075/epfl-298799_978-2-9701614-0-0

nanoparticles (graphene platelets, carbon nanotubes, etc.) in enhancing the mechanical and multifunctional properties of polymers [7,8]. Various studies of CNT reinforced polymers have shown improved toughness over the neat matrix [9–11] inducing toughening mechanisms, such as crack deflection [12], crack pinning [11], CNT pull-out [13,14], microscale and nanoscale crack bridging [15]. However, these mechanisms require some degree of interaction between the crack front and the CNTs. Recent studies postulate the benefits of adding nanoparticles in a targeted fashion with controlled nanoparticle network morphology to trigger/activate multiscale damage suppression events as opposed to the less effective technique of homogenously dispersing the nanoparticles in a host polymer [12,16].

In this study, the authors explore the role of interleaf films containing CNT only in co-cured interfaces to delay and diffuse damage propagation [17,18] by allowing the CNT to directly interact with the crack front. This targeted reinforcement approach is preferred over the option to disperse the CNT in the entire matrix phase of the composite. A related previous study involving molecular simulations of CNT-dispersed matrix showed that elastic mechanical properties of the nanocomposite can be improved by adding CNT up to 2% wt. Loading levels beyond 2% wt. were shown to interfere with the epoxy crosslinking process and lead to deterioration of mechanical properties [19]. Therefore, we investigate CNT loading levels up to 2% wt. in the epoxy used for interleaving and consider two different interleaf thicknesses and their combined effects on damage propagation mechanisms.

Motivated by the effectiveness of nano-interleaves on toughening composite interfaces and their potential for expanded applications in co-cured composite joints, this study investigates the damage mechanisms in the interleaved interface from experiments performed under mode I load with double cantilever beam (DCB) specimens. The main parameters studied are the nanoparticle concentration and interleaf thickness. Following the mechanical tests, in order to investigate the type of interfacial failure (adhesive/cohesive), microcracking in the interleaf, and migration of the crack path, the fracture surfaces were examined with optical and confocal microscopes.

2. Experimental Work

2.1 Materials

The prepreg used for this study was unidirectional carbon IM7 fiber with HexPly® 8552 epoxy resin system of ply thickness 0.13 *mm*. Neat epoxy interleaves (containing no nanoparticles) in the study were manufactured with the API-60 epoxy system – an aerospace grade resin – purchased from Kaneka Aerospace Inc. with a compatible thermal cure cycle and properties with the HexPly® 8552 proprietary resin system. Filmed interleaves containing multi-walled CNT were procured from NanoSperse with the same host epoxy matrix at three nanoparticle concentrations (0.5% wt., 1% wt., 2% wt.) and two interleaf thicknesses (200 μ and 500 μ).

2.2 Laminate manufacturing with interleaves

All laminate specimens in the study consist of a [$0°_{12}$/interleaf/$0°_{12}$] lay-up and a unidirectional fracture interface. Both the neat epoxy interleaf as well as the CNT interleaves are staged (semi-cured) in the oven, subsequent to their complete cure kinetics characterization [3], to attain a resulting degree of cure between 0.3 – 0.35. An initial delamination is embedded in the laminate

spanning 35 *mm* using a Teflon release film of 25 *μ* thickness. During the laminate consolidation process, the interleaf film was introduced at the edge where the Teflon delamination insert ended. Figure 1 shows the staged interleaves and their consolidation into the laminate, which was cured in the autoclave according to the recommended prepreg cure cycle. The cured plates were trimmed and cut into samples of approximately 150 - 160 *mm* in length and 25 *mm* in width with a diamond-tipped circular saw for the fracture toughness tests. It must be noted that the total length of the actual specimen does not affect the test results as long as it is over 100 *mm*. The thickness of the specimens varied between 3.3 and 3.8 *mm* depending on the embedded interleaf thickness.

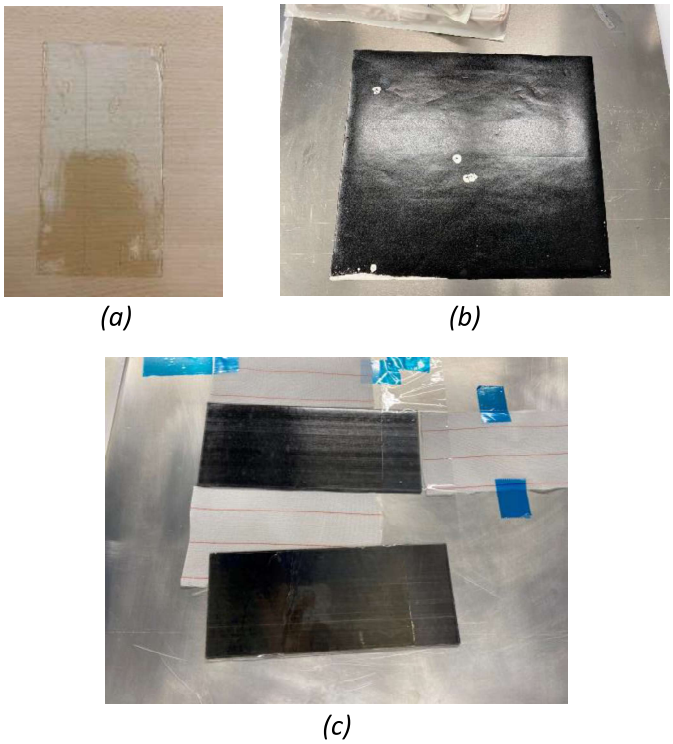

Figure 1. Manufacturing and consolidation of the laminate with interleaved interface (a) Neat epoxy interleaf (200 *μ thickness); (b) CNT interleaf (0.5% wt., 200 μ thickness); (c) integration of interleaf in the laminate midplane*

2.3 Test setup and analysis scheme

Double cantilever beam samples were tested in mode I loading conditions conforming to ASTM standards [20] to calculate fracture toughness values and resistance effects to damage propagation. The samples tested and their corresponding nomenclature in the rest of this paper are reported in Table 1. All fracture tests were performed on a Zwick tension/compression test frame with 10 *kN* maximum capacity. The load frame was attached to a 1 *kN* load cell for the DCB tests. The samples were painted white, and 1 *mm* markings were made in black ink to track crack length propagation. Images from two monochromatic cameras perpendicular of the longitudinal axis of the samples were acquired every second to monitor crack length. Images from the two cameras were also helpful to determine if the crack front is asymmetric resulting in different crack lengths on either side.

  doi:10.5075/epfl-298799_978-2-9701614-0-0

Table 1. Number of samples and nomenclature based on interleaf type and thickness

Plate no.	Interleaf thickness [μ]	CNT conc. [% wt.]	Nomenclature	No. of samples
1	200	0 (Neat)	Neat200μDCB	2
2	200	0.5	0.5%CNT200μDCB	3
3	500	0.5	0.5%CNT500 μDCB	3
4	200	1	1%CNT200μDCB	3
5	500	1	1%CNT500μDCB	3
6	200	2	2%CNT200μDCB	3
7	500	2	2%CNT500μDCB	3

Figure 2 illustrates the mode I test with a piano hinge bonded to the sample. The samples in mode I were loaded at a constant crosshead displacement of 0.3 *mm/min.* It was expected as well as confirmed with subsequent microscopy that the limited flow of the interleaf epoxy during the cure cycle would allow for the crack front to be in contact with the interleaf layer. But a sharp and straight crack front with every point fully embedded in the interleaf layer could not be verified. Therefore, all samples were pre-cracked using the prescribed pre-cracking technique in ASTM D5528 to achieve an initial crack length between 28 and 32 *mm*.

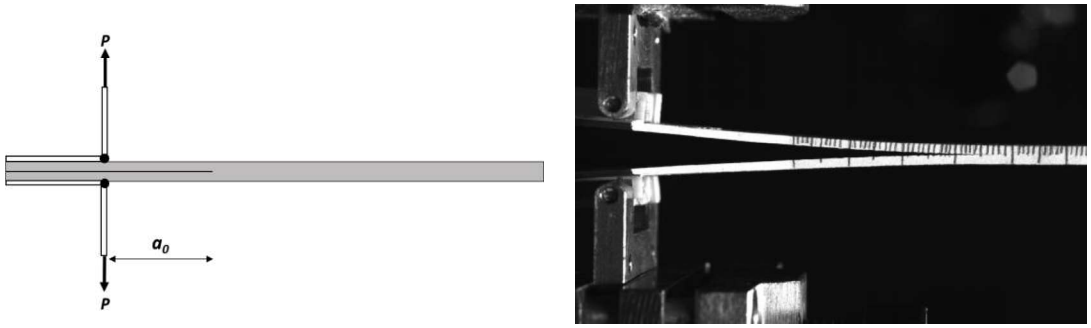

(a) *(b)*

Figure 2. Test setup for mode I fracture toughness testing (a) schematic of the DCB sample test with piano hinges; (b) image captured from monochromatic camera of DCB sample

Data reduction to compute mode I fracture toughness is performed on the load-displacement *(P-δ)* data from the test machine as well as the crack lengths from the captured images using the modified compliance calibration (MCC) approach [21]. This approach is chosen because it allows to account for the thickness differences among the samples while calculating mode I fracture toughness (G_I). A least squared plot of the crack length normalized by sample thickness *(a/h)* as a function of the cube root of compliance $(C^{1/3})$ is generated and the slope of this fit corresponds to A_1; *P is the load and b* is the sample width. The critical initiation fracture toughness (G_{Ic}) is computed by using the critical load (P_{crit}) instead of *P* in Eq. (1).

$$G_I = \frac{3P^2\, C^{2/3}}{2A_1 bh} \tag{1}$$

3. Results and Discussion

The load-displacement data obtained from the Zwick test frame for a representative sample from each set (described in Table 1) are plotted in Figure 3. The data is categorized based on the nanoparticle content and compared to the neat epoxy interleaved laminate in each case. While the *P-δ* profile of the neat epoxy interleaved interface indicates a stable, typical crack propagation, the inclusion of nanoparticles to the interface remarkably alters the damage mechanisms. In each case, the addition of nanoparticles leads to a significant improvement in the flexural stiffness of the sample. The slope of the linear *P-δ* section remains fairly constant for a specific CNT wt. content but appears to increase with increasing CNT content. The saw-tooth profiles in Figure 3 imply unstable crack growth followed by a strong arrest mechanism. The peak of each saw-tooth corresponds to the initiation load to propagate the crack at that specific crack length; however, the troughs of the saw-tooth indicate an arrest mechanism, subsequent to which the sample continues to behave 'elastically' with a reduced stiffness but no change to the crack length, until the next initiation load. The overall strain energy (area under the curve) is higher than the baseline laminate (with neat epoxy interleaf) even at low wt. contents of CNT.

The damage propagation in mode I for CNT interleaved interfaces can be described by a 'slip-stick' mechanism [22] as illustrated in Figure 4, where each sudden load drop in Figure 3 results in a crack slip/jump (sudden increase in crack length) but this slip is then arrested by a 'stick' phenomenon and held intact until the next slip event. The higher the load drop, the larger the crack slip tends to be. Although the mechanism of damage propagation is altered, the forces for crack arrest (troughs of the saw-tooth) are consistent with the forces in the baseline laminate containing the same interleaf thickness, i.e., each CNT interleaved laminate containing a 200 μ interleaf possesses a *P-δ* profile that falls to the baseline laminate *P-δ* profile at the end of a crack slip event.

Interleaf thickness exhibits a significant effect on the peak initiation loads, arrest loads, as well as the overall strain energy of the samples. As mentioned earlier, the thickness of the interleaf with no nanoparticles (neat epoxy) determines the lower bound for the *P-δ* profile when nanoparticles are added to the interface. Comparing the laminates with the same CNT wt. content but different interleaf thicknesses (Figures 4 (a)-(c)), it can be noted that the slip events are 'delayed' in the interfaces containing a thicker interleaf. This is demonstrated by the fact that each load drop in the *P-δ* curve occurs at a higher displacement for the 500 μ interleaved samples when compared to their thinner interleaved equivalent.

Micrographs obtained via a Zeiss Keyence Wide-angle laser microscope, as shown in Figure 5, also display higher tortuosity to the crack path and undulations in the interface for thicker interleaves. The undulations in the micrographs confirm cohesive-dominated failure in the thicker interleaf while suggesting a mix of adhesive and cohesive failure regions in Figure 5(a) as illustrated by regions of adhesive peeling [23]. Furthermore, Figure 5(b) reveals that the waviness of the undulations are clustered close to the mid-line (shorter wave-lengths) and they become sparser (with longer wave-lengths) towards the edge of the specimen. This indicates that the delamination front is not a straight line but curved and quasi-parabolic. The striations as well as the post-processed images from both cameras confirm that the crack length is nearly equal on both edges during the test thus implying that the quasi-parabolic crack front is symmetric [24].

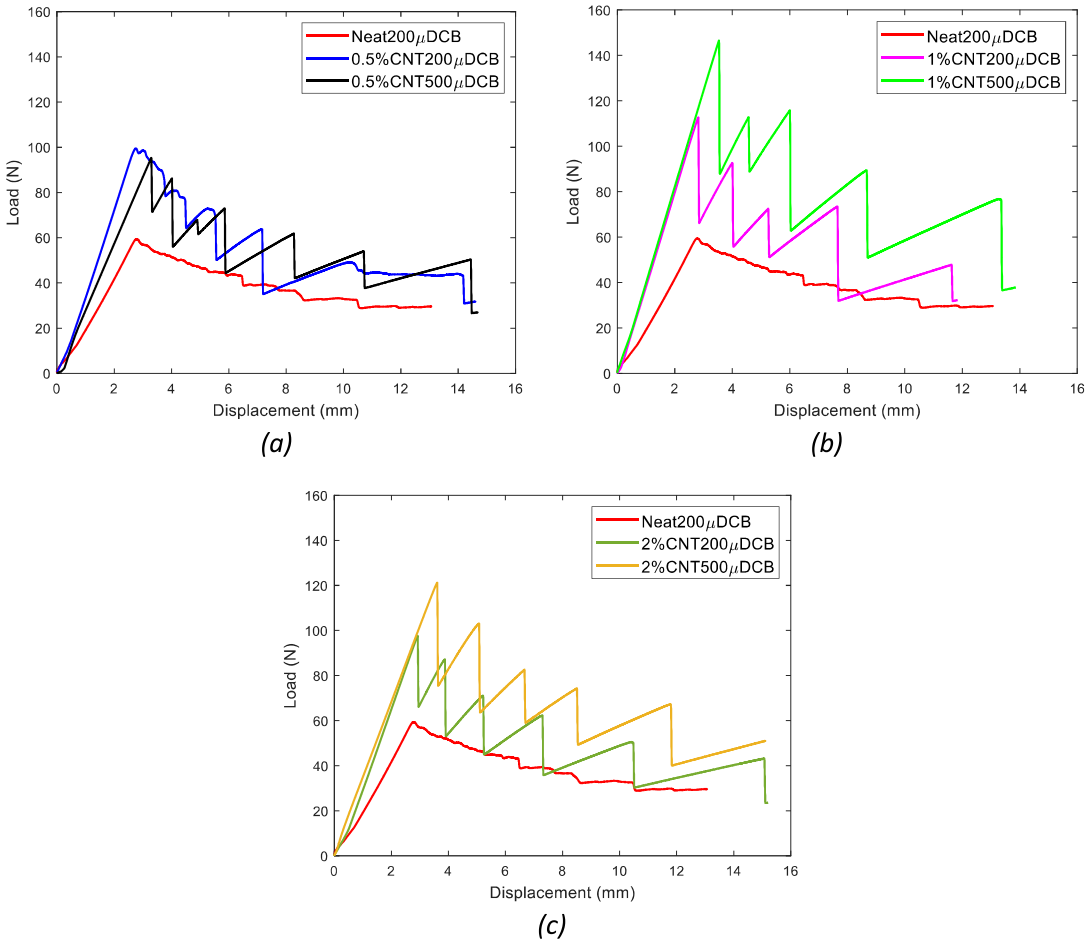

Figure 3. Comparison of load-displacement curves from DCB tests with neat epoxy interleaved interface (a) 0.5% CNT interleaves; (b) 1% CNT interleaves; (c) 2% CNT interleaves

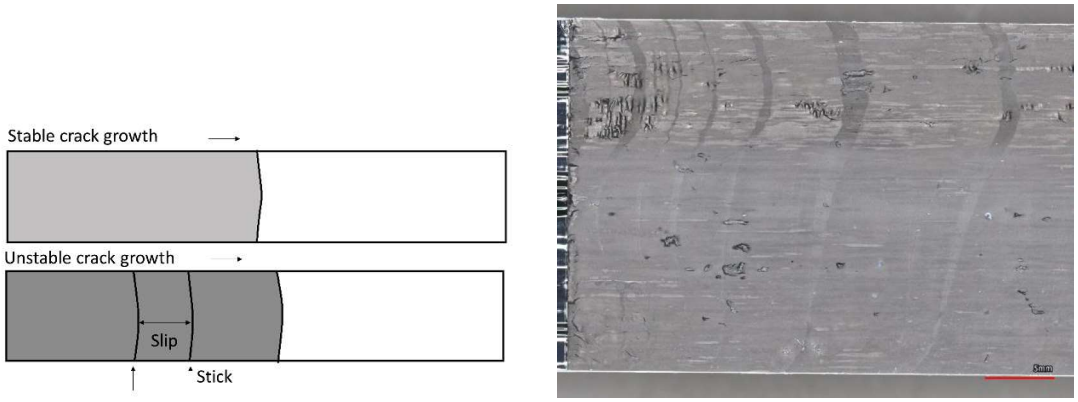

Figure 4. Slip-stick damage propagation (a) schematic of the fracture surface; (b) micrograph of failure surface from 1%CNT200μDCB with slip-stick striations

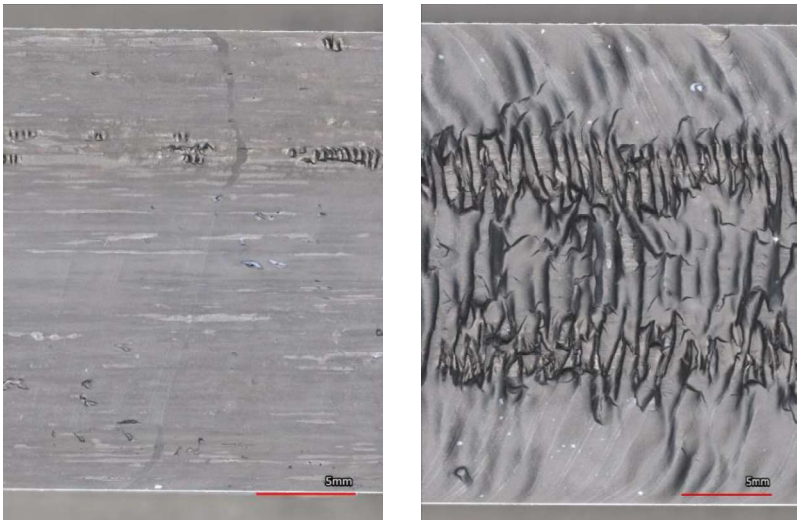

(a) *(b)*

Figure 5. Fracture striations and undulations on failed surface (a) in 1%CNT200µDCB; (b) in 1%CNT500µDCB

Data in literature places the critical mode I fracture toughness for IM7/8552 composites in the 0.2 – 0.23 kJ/m^2 range [25]. A larger spread is observed (between 0.2 – 0.27 kJ/m^2) [26] when using different approaches to determine the critical load (P_{crit}) in Eq. (1) such as visually observed deviation from linearity, or the 5% offset method described in ASTM D5528. Composite interfaces also exhibit a toughening effect to crack propagation owing to fiber bridging ahead of the crack front, represented generally with R-curves. As the crack length increases, more energy is required to further propagate the crack due to pinning and bridging effects between the fibers. The R-curves in Figure 6 contain mean fracture toughness values from multiple samples (as described in Table 1) in a sample set. In this study, the presence of an interleaf region does not allow for microscale fiber bridging across the fracture interface thus resulting in no R-curve effect.

A neat epoxy interleaf interacting with the crack front improves the mode I initiation resistance to the range: 0.25 – 0.3 kJ/m^2 [3] according to a previous study by the authors. In this batch of samples, however, no statistical difference between the neat epoxy interleaved interface and a laminate with no interleaf is observed here. Another remarkable characteristic of interleaved interfaces is the absence of any additional resistance as the crack length increases. The R-curves remain fairly flat in all cases although significant gains in toughness are observed as a result of the addition of CNT to the interleaves. We observe no statistically significant difference between laminates containing varying concentrations of CNT within a 200 μ interleaf. This indicates that toughening mechanisms in mode I are more sensitive/responsive to the thickness of the interleaf than the concentration of nanoparticles. Toughness of the interleaved laminate improves up to nearly 4 times with CNT concentrations ≥1% and an interleaf thickness of 500 μ.

The test data and micrograph striations demonstrate a crack arrest mechanism in CNT-interleaved laminates. This arrest seems to occur at a load nearly equal to that of a neat epoxy interleaved laminate of the same interleaf thickness. Therefore, a neat epoxy interleaf appears to set the lower bound for the force-displacement profile of a CNT-interleaved laminate. At

  doi:10.5075/epfl-298799_978-2-9701614-0-0

higher CNT wt. %, we observe higher initiation loads but larger load drops (corresponding to larger crack jumps), whereas increasing interleaf thickness shifts the load drop events (slip) to higher displacements indicating a damage delay mechanism. The *P-δ* data and the micrographs affirm that crack growth processes are altered at two scales due to nanoparticle interleaving: at the macroscale via slip-stick based jump and via microscale tortuosity behind the quasi-parabolic crack front.

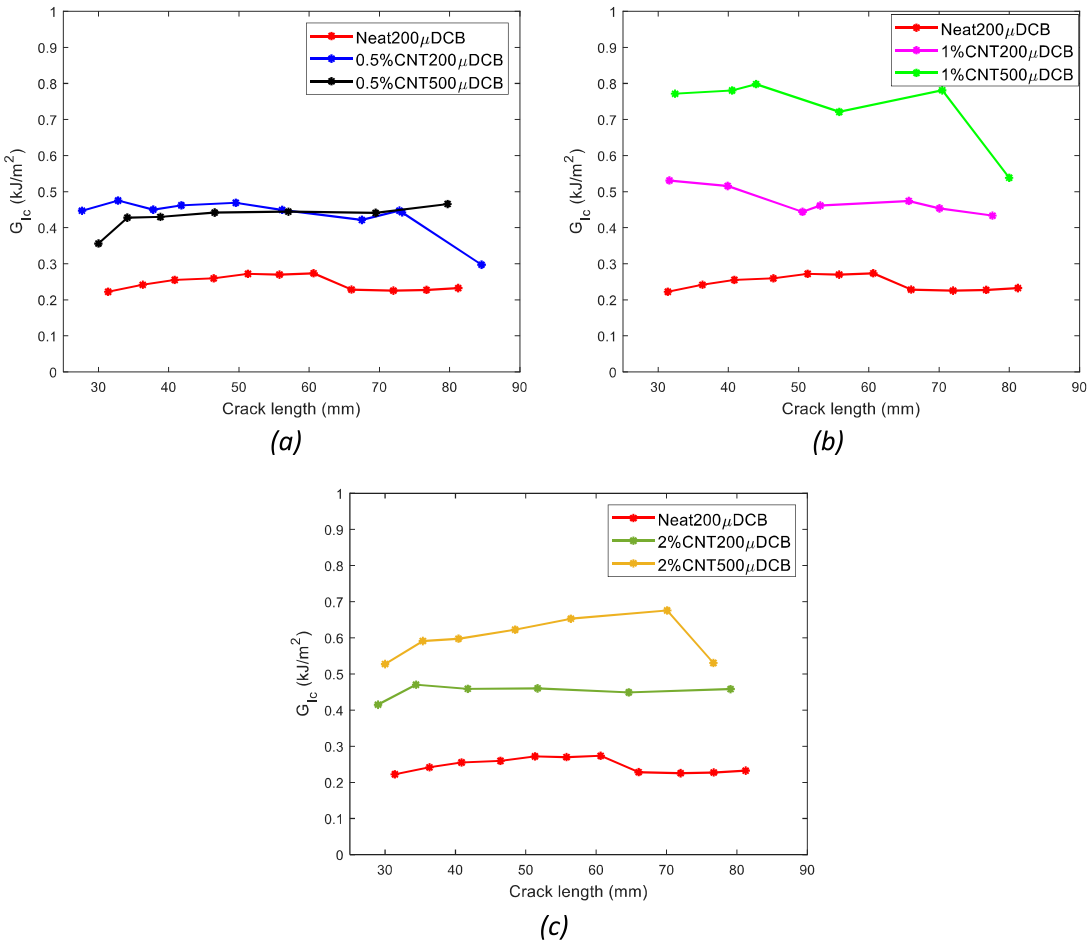

Figure 6. R-curves from DCB tests compared with neat epoxy interleaved interface (a) 0.5% CNT interleaves; (b) 1% CNT interleaves; (c) 2% CNT interleaves

4. Conclusions

This study was focused on the incorporation of semi-cured interleaves containing nanoparticles in the composite consolidation process and its effectiveness in mode I fracture resistance. Interleaves with neat epoxy as well as different concentrations of CNT were staged to a predefined degree of cure to maintain their integrity and thickness during consolidation into the laminate. Interleaves of two different thicknesses were considered in this study. The double cantilever beam samples prepared using this approach were tested under mode I loading.

The load-displacement data as well as micrographs of failed surfaces revealed a remarkable change in the underlying damage mechanisms governing crack propagation in mode I. The

  doi:10.5075/epfl-298799_978-2-9701614-0-0

addition of nanoparticles to the interleaf resulted in a higher flexural stiffness of the sample whereas the critical fracture initiation loads were more sensitive to interleaf thickness. A slip-stick phenomenon was observed with damage progression where the crack arrest load for a CNT interleaf could be predicted by the load-displacement profile of a neat epoxy interleaf of same thickness. Improvements in mode I fracture toughness of up to 4 times were observed with the inclusion of CNT within a thicker 500 μ interleaf when compared to a baseline interleaf without nanoparticles. There is no significant resistance behaviour (R-curve effects) to crack propagation as a function of crack length as no bridging effects were observed. Data from the fracture toughness tests were augmented with wide-angle microscopy of the fractured surfaces to shed light on crack front progression and the microscale mechanisms that lead to damage delay.

Acknowledgements

This project has received funding from the European Union's Horizon 2020 research and innovation programme under the Marie Skłodowska-Curie grant agreement No. 835672. The authors acknowledge the support from the Delft Aerospace Materials and Structures Lab (DASML), particularly Alexander Uithol, to conduct experiments and post-process image data.

5. References

[1] Mohan, J., Ivanković, A., and Murphy, N. "Mode I Fracture Toughness of Co-Cured and Secondary Bonded Composite Joints." *International Journal of Adhesion and Adhesives*, Vol. 51, 2014, pp. 13–22.

[2] Brito, C. B. G., Contini, R. de C. M. S., Gouvêa, R. F., Oliveira, A. S. de, Arbelo, M. A., and Donadon, M. V. "Mode I Interlaminar Fracture Toughness Analysis of Co-Bonded and Secondary Bonded Carbon Fiber Reinforced Composites Joints." *Materials Research*, Vol. 20, No. suppl 2, 2018, pp. 873–882.

[3] Subramanian, N., and Bisagni, C. Multiscale damage in co-cured composites—perspectives from experiments and modelling. Presented at the Thirty-sixth Technical Conference, 2021.

[4] Chen, S. F., and Jang, B. Z. "Fracture Behaviour of Interleaved Fiber-Resin Composites." *Composites Science and Technology*, Vol. 41, No. 1, 1991, pp. 77–97.

[5] Marino, S. G., and Czél, G. "Improving the Performance of Pseudo-Ductile Hybrid Composites by Film-Interleaving." *Composites Part A: Applied Science and Manufacturing*, Vol. 142, 2021, p. 106233.

[6] Singh, S., and Partridge, I. K. "Mixed-Mode Fracture in an Interleaved Carbon-Fibre/Epoxy Composite." *Composites Science and Technology*, Vol. 55, No. 4, 1995, pp. 319–327.

[7] Avilés, F., Oliva-Avilés, A. I., and Cen-Puc, M. "Piezoresistivity, Strain, and Damage Self-Sensing of Polymer Composites Filled with Carbon Nanostructures." *Advanced Engineering Materials*, Vol. 20, No. 7, 2018, p. 1701159.

[8] Rai, A., Subramanian, N., and Chattopadhyay, A. Investigation of Piezo-Resistivity in CNT Nano-Composites under Damage. Presented at the SPIE Smart Structures and Materials + Nondestructive Evaluation and Health Monitoring, Las Vegas, Nevada, United States, 2016.

[9] Zainol Abidin, M. S., Herceg, T., Greenhalgh, E. S., Shaffer, M., and Bismarck, A. "Enhanced Fracture Toughness of Hierarchical Carbon Nanotube Reinforced Carbon Fibre Epoxy Composites with Engineered Matrix Microstructure." *Composites Science and Technology*, Vol. 170, 2019, pp. 85–92.

[10] Wichmann, M. H. G., Schulte, K., and Wagner, H. D. "On Nanocomposite Toughness." *Composites Science and Technology*, Vol. 68, No. 1, 2008, pp. 329–331.

  doi:10.5075/epfl-298799_978-2-9701614-0-0

[11] Wetzel, B., Rosso, P., Haupert, F., and Friedrich, K. “Epoxy Nanocomposites – Fracture and Toughening Mechanisms.” *Engineering Fracture Mechanics*, Vol. 73, No. 16, 2006, pp. 2375–2398.

[12] Liu, Q., Lomov, S. V., and Gorbatikh, L. “The Interplay between Multiple Toughening Mechanisms in Nanocomposites with Spatially Distributed and Oriented Carbon Nanotubes as Revealed by Dual-Scale Simulations.” *Carbon*, Vol. 142, 2019, pp. 141–149.

[13] Rai, A., Subramanian, N., Koo, B., and Chattopadhyay, A. “Multiscale Damage Analysis of Carbon Nanotube Nanocomposite Using a Continuum Damage Mechanics Approach.” *Journal of Composite Materials*, Vol. 51, No. 6, 2017, pp. 847–858.

[14] Subramanian, N. *Physics-Based Modeling of Material Behavior and Damage Initiation in Nanoengineered Composites*. Doctoral Dissertation Aerospace Engineering 2018. Arizona State University, Tempe, Arizona, USA, 2018.

[15] Garcia, E. J., Wardle, B. L., and John Hart, A. “Joining Prepreg Composite Interfaces with Aligned Carbon Nanotubes.” *Composites Part A: Applied Science and Manufacturing*, Vol. 39, No. 6, 2008, pp. 1065–1070.

[16] Liu, Q., Lomov, S. V., and Gorbatikh, L. “Enhancing Strength and Toughness of Hierarchical Composites through Optimization of Position and Orientation of Nanotubes: A Computational Study.” *Journal of Composites Science*, Vol. 4, No. 2, 2020, p. 34.

[17] Warren, Graham Leicester. *EPOXY/SINGLE WALLED CARBON NANOTUBE NANOCOMPOSITE THIN FILMS FOR COMPOSITES REINFORCEMENT*. Texas A&M University, 2009.

[18] Shin, Y. C., Lee, W. I., and Kim, H. S. “Mode II Interlaminar Fracture Toughness of Carbon Nanotubes/Epoxy Film-Interleaved Carbon Fiber Composites.” *Composite Structures*, Vol. 236, 2020, p. 111808.

[19] Subramanian, N., Rai, A., and Chattopadhyay, A. “Atomistically Informed Stochastic Multiscale Model to Predict the Behavior of Carbon Nanotube-Enhanced Nanocomposites.” *Carbon*, Vol. 94, 2015, pp. 661–672.

[20] D30 Committee. *Test Method for Mode I Interlaminar Fracture Toughness of Unidirectional Fiber-Reinforced Polymer Matrix Composites*. ASTM International.

[21] Kageyama, K., and Hojo, M. Proposed Methods for Interlaminar Fracture Toughness Tests of Composite Laminates. Presented at the Achievement in composites in Japan and the United States, 1990.

[22] Zhou, Y., Xiao, Y., Wu, Q., and Xue, Y. “A Multi-State Progressive Cohesive Law for the Prediction of Unstable Propagation and Arrest of Mode-I Delamination Cracks in Composite Laminates.” *Engineering Fracture Mechanics*, Vol. 248, 2021, p. 107684.

[23] Silveira, N. N. A., Sales, R. C. M., Brito, C. B. G., Cândido, G. M., and Donadon, M. V. “Comparative Fractographic Analysis of Composites Adhesive Joints Subjected to Mode I Delamination.” *Polymer Composites*, Vol. 40, No. 8, 2019, pp. 2973–2983.

[24] Guo, S., Xia, Y., Wei, X., and Zhou, Q. “Investigation on the Stable and Stick-Slip Crack Propagation Behaviors in Double Cantilever Beam Test.” *The Journal of Adhesion*, Vol. 96, No. 13, 2020, pp. 1198–1218.

[25] Krueger, R. “A Summary of Benchmark Examples to Assess the Performance of Quasi-Static Delamination Propagation Prediction Capabilities in Finite Element Codes.” *Journal of Composite Materials*, Vol. 49, No. 26, 2015, pp. 3297–3316.

[26] Raimondo, A., Urcelay Oca, I., and Bisagni, C. “Influence of Interface Ply Orientation on Delamination Growth in Composite Laminates.” *Journal of Composite Materials*, No. in press, 2021.

